Effect of natural iron fertilization on carbon sequestration in the Southern Ocean

Stéphane Blain, Bernard Queguiner, Leanne Armand, Sauveur Belviso, Bruno Bombled, Laurent Bopp, Andrew R. Bowie, Christian Brunet, Corina Brussaard, Francois Carlotti, et al.

▶ **To cite this version:**

Stéphane Blain, Bernard Queguiner, Leanne Armand, Sauveur Belviso, Bruno Bombled, et al.. Effect of natural iron fertilization on carbon sequestration in the Southern Ocean. Nature, 2007, 446 (7139), pp.1070-1075. 10.1038/nature05700 . hal-00169813

HAL Id: hal-00169813
https://hal.science/hal-00169813

Submitted on 4 Dec 2022

HAL is a multi-disciplinary open access archive for the deposit and dissemination of scientific research documents, whether they are published or not. The documents may come from teaching and research institutions in France or abroad, or from public or private research centers.

L'archive ouverte pluridisciplinaire **HAL**, est destinée au dépôt et à la diffusion de documents scientifiques de niveau recherche, publiés ou non, émanant des établissements d'enseignement et de recherche français ou étrangers, des laboratoires publics ou privés.

Distributed under a Creative Commons Attribution - NonCommercial 4.0 International License

Effect of natural iron fertilization on carbon sequestration in the Southern Ocean

Stéphane Blain[1], Bernard Quéguiner[1], Leanne Armand[1], Sauveur Belviso[2], Bruno Bombled[2], Laurent Bopp[2], Andrew Bowie[3,4], Christian Brunet[5], Corina Brussaard[6], François Carlotti[1], Urania Christaki[7], Antoine Corbière[5], Isabelle Durand[8], Frederike Ebersbach[3], Jean-Luc Fuda[9], Nicole Garcia[1], Loes Gerringa[6], Brian Griffiths[10], Catherine Guigue[11], Christophe Guillerm[12], Stéphanie Jacquet[13], Catherine Jeandel[14], Patrick Laan[6], Dominique Lefèvre[11], Claire Lo Monaco[5], Andrea Malits[15], Julie Mosseri[1], Ingrid Obernosterer[16], Young-Hyang Park[8], Marc Picheral[15], Philippe Pondaven[17], Thomas Remenyi[3], Valérie Sandroni[1], Géraldine Sarthou[17], Nicolas Savoye[13,18], Lionel Scouarnec[12], Marc Souhaut[14], Doris Thuiller[5], Klaas Timmermans[6], Thomas Trull[3,10], Julia Uitz[15], Pieter van Beek[14], Marcel Veldhuis[6], Dorothée Vincent[7], Eric Viollier[19], Lilita Vong[1] & Thibaut Wagener[15]

The availability of iron limits primary productivity and the associated uptake of carbon over large areas of the ocean. Iron thus plays an important role in the carbon cycle, and changes in its supply to the surface ocean may have had a significant effect on atmospheric carbon dioxide concentrations over glacial–interglacial cycles[1–5]. To date, the role of iron in carbon cycling has largely been assessed using short-term iron-addition experiments[6,7]. It is difficult, however, to reliably assess the magnitude of carbon export to the ocean interior using such methods, and the short observational periods preclude extrapolation of the results to longer timescales[8]. Here we report observations of a phytoplankton bloom induced by natural iron fertilization—an approach that offers the opportunity to overcome some of the limitations of short-term experiments. We found that a large phytoplankton bloom over the Kerguelen plateau in the Southern Ocean was sustained by the supply of iron and major nutrients to surface waters from iron-rich deep water below. The efficiency of fertilization, defined as the ratio of the carbon export to the amount of iron supplied, was at least ten times higher than previous estimates from short-term blooms induced by iron-addition experiments[7]. This result sheds new light on the effect of long-term fertilization by iron and macronutrients on carbon sequestration, suggesting that changes in iron supply from below—as invoked in some palaeoclimatic[9,10] and future climate change scenarios[11]—may have a more significant effect on atmospheric carbon dioxide concentrations than previously thought.

The Southern Ocean plays a major role in the climate system, and is recognized as the oceanic body most sensitive to climate change[12,13]. Iron fertilization of its surface waters during glacial times by enhanced dust deposition is a scenario (known as the 'iron hypothesis'[1]) proposed to explain lower atmospheric CO_2 during colder climates. Different versions of this scenario[2,3], as well as the magnitude of the CO_2 drawdown induced by iron fertilization[4,5], are still debated, but the important role of iron in carbon cycling is no longer in question. The proximate control of biological productivity by iron in the Southern Ocean has been unequivocally demonstrated by iron addition experiments[14–16]. All experiments show an enhancement of primary production associated with a shift in the structure of the phytoplankton community[7]. However, the short observational periods, as well as other intrinsic limits and artefacts of the small scale fertilization technique, have prevented a clear assessment of carbon export and preclude extrapolation to longer timescales.

Although the Southern Ocean is the largest high-nutrient low-chlorophyll (HNLC) region of the global ocean, natural phytoplankton blooms do occur in the vicinity of many Southern Ocean islands, as first reported in ref. 17 and subsequently characterized in detail by satellite images[18,19]. The largest bloom is observed around Kerguelen Island and the adjacent plateau to its southeast (Fig. 1a, b). The bloom has two main features: (1) a narrow plume that extends northeast of the island and north of the Polar Front that shows high mesoscale and temporal variability[20], and (2) a larger bloom ($\sim$45,000 km^2) southeast of the island and south of the Polar Front which is remarkably constrained to the bathymetry of the plateau. In 2004–05, this larger bloom began in early November, achieved high phytoplankton biomass ($\sim$3 μg chlorophyll *a* per litre) in December and January and then collapsed in late February (Fig. 1c).

The KEOPS (Kerguelen ocean and plateau compared study; 19 January to 13 February 2005) cruise carried out a survey inside and outside this bloom (Fig. 1b), with particular focus on two contrasting stations: A3 (50° 38′ S, 72° 05′ E) and C11 (51° 39′ S, 78° 00′ E).

[1]Laboratoire d'Océanographie et de Biogéochimie, Centre Océanologique de Marseille, CNRS, Université de la Méditerranée, campus de Luminy, case 901, 13288 Marseille Cedex 09, France
[2]IPSL/Laboratoire des Sciences du Climat et de l'Environnement, CEN de Saclay, Bât. 701 l'Orme des Merisiers, 91191 Gif-sur-Yvette, France.
[3]Antarctic Climate and Ecosystems CRC, Hobart, Tasmania 7001, Australia.
[4]ACROSS, School of Chemistry, University of Tasmania, Hobart, Tasmania 7001, Australia.
[5]LOCEAN-IPSL, UMR 7159, CNRS, Université P. et M. Curie, Case 100, 4 place Jussieu, 75252 Paris Cedex 5, France.
[6]Royal Netherlands Institute for Sea Research (NIOZ), PO Box 59, 1790 AB Den Burg, Texel, The Netherlands.
[7]FRE ELICO, Université du Littoral Coˆte d'Opale, Maison de la Recherche en Environnement Naturel (MREN), 32 avenue Foch, 62930 Wimereux, France.
[8]USM402/LOCEAN, Département des Milieux et Peuplements Marins, Muséum National d'Histoire Naturelle, 43 rue Cuvier, F-75231 Paris Cedex 05, France.
[9]Centre Océanologique de Marseille, Campus de Luminy, 13288 Marseille Cedex 09, France.
[10]CSIRO Division of Marine and Atmospheric Research, GPO Box 1538, Hobart, Tasmania 7001, Australia.
[11]LMGEM UMR CNRS 617, Campus de Luminy, case 901, 13288 Marseille Cedex 09, France.
[12]DT INSU CNRS, Bâtiment IPEV BP 74, Technopole Brest Iroise, 29280 Plouzané, France.
[13]Department of Analytical and Environmental Chemistry, Vrije Universiteit Brussel, Pleinlaan 2, B-1050 Brussels, Belgium.
[14]LEGOS (CNRS/CNES/IRD/UPS), Observatoire Midi-Pyrénées, 14 avenue Edouard Belin, 31400 Toulouse, France.
[15]Laboratoire d'Océanographie de Villefranche, Quai de La Darse, BP 8, 06238 Villefranche-sur-Mer, France.
[16]Université Pierre et Marie Curie-Paris 6, UMR7621, CNRS, F66650 Banyuls-sur-Mer, France.
[17]UMR 6539/LEMAR/IUEM, Technopole Brest Iroise, Place Nicolas Copernic, 29280 Plouzané, France.
[18]Observatoire Aquitain des Sciences de l'Univers, UMR CNRS 5805 EPOC, Station Marine d'Arcachon, 2 rue du Pr. Jolyet, 33120 Arcachon, France.
[19]Laboratoire de Géochimie des Eaux, UMP IPGP 7154, Université Denis Diderot Paris 7, 2 place Jussieu, 75251 Paris Cedex 05, France.

Measurements of the partial pressure of CO_2 (p_{CO_2}) in surface waters indicate that the bloom was an important sink for CO_2 (Fig. 1d), with a mean p_{CO_2} drawdown of 58 ± 11 µatm, which was ~2–3 times higher than that observed following Southern Ocean iron addition experiments, probably reflecting the longer duration of the Kerguelen bloom. Silicic acid was almost depleted (1–2 µM), while nitrate concentrations remained relatively high (23 µM) (Supplementary Fig. 1).

Measurements of dissolved iron (DFe) revealed that concentrations in the surface mixed layer were low on and off the plateau (0.090 ± 0.034 nM; mean ± s.d., $n = 49$) and typical of surface waters of the open Southern Ocean[15,21]. But vertical profiles of DFe revealed a major difference between on- and off-plateau stations below 150 m (Fig. 2b). Above the plateau, DFe concentrations increased with depth and reached a mean maximum of ~0.35 nM (range 0.19–0.51 nM) at 500 m, close to the bottom. In contrast, off the plateau (bottom > 1,500 m) mean DFe concentrations were ~0.18 nM at 600 m. Organic ligand concentrations (L) were sufficient to keep the supplied DFe soluble (L/DFe > 2.4 for all stations). The low concentrations of DFe measured in surface waters both on and off the plateau are known to be close to rate-limiting for many phytoplankton from bottle[22] and mesoscale iron addition experiments[14–16]. Thus it appears that phytoplankton production depletes the iron to rate-limiting levels both off and on the plateau, with the higher biomass over the plateau induced by higher iron supply from below.

Availability of iron in surface waters over the plateau appears to be enhanced by the greater winter stock and by a higher ongoing supply from increased vertical mixing and the steeper DFe gradient. Between 100 and 200 m, the vertical diffusivity ($K_z = (3.3 \pm 3.3) \times 10^{-4}\ m^2\ s^{-1}$, see Table 1) was substantially higher than the most recent estimate of K_z in the open Southern Ocean ($(0.11 \pm 0.2) \times 10^{-4}\ m^2\ s^{-1}$)[23]. This enhancement of vertical mixing was probably due to internal wave activity (Fig. 2c, d), which also appears to enhance mixing at the C11 site off the plateau ($K_z = (3.2 \pm 2.3) \times 10^{-4}\ m^2\ s^{-1}$, see Table 1). Combining the K_z estimates with the DFe gradients (Table 1) suggests a nearly eightfold higher DFe flux into surface waters on the plateau (31 nmol $m^{-2}\ d^{-1}$) than off the plateau (4 nmol $m^{-2}\ d^{-1}$). For comparison, DFe fluxes around 3 nmol $m^{-2}\ d^{-1}$ were found at the SOIREE and FeCycle HNLC sites[23,24].

The net DFe requirements of phytoplankton (208 ± 77 nmol $m^{-2}\ d^{-1}$)—defined as the difference between the total uptake and regeneration rates of DFe, and estimated from our ^{55}Fe experiments carried out at the beginning (19 January) and at the end (12 February) of the survey—are not balanced by the vertical supply of DFe (31 nmol $m^{-2}\ d^{-1}$). This suggests an additional supply from, for example, ongoing depletion of the winter surface stock or from dissolution of lithogenic particulate Fe (PFe_{litho}). The total supply cannot exceed the demand, because this would lead to elevated iron concentrations in surface waters that would be in contradiction with our observations. Between 19 January and 12 February, the steady depletion of a winter stock by 0.06 nM or the application of a daily dissolution rate of ~2.5% of the observed PFe_{litho} at A3 on 24 January (~0.1 nM based on particulate Al and a crustal Fe/Al ratio) is sufficient to balance the demand. The accurate determination of these fluxes is out of reach of the present analytical capabilities, but the values are within realistic ranges[11] and are upper limits because the additional supply is most probably a combination of both processes. Constraining the balance of the demand with supply suggests an additional DFe input of 177 nmol $m^{-2}\ d^{-1}$ at A3 (Table 1). Including this possible supply suggests an excess of DFe supply over

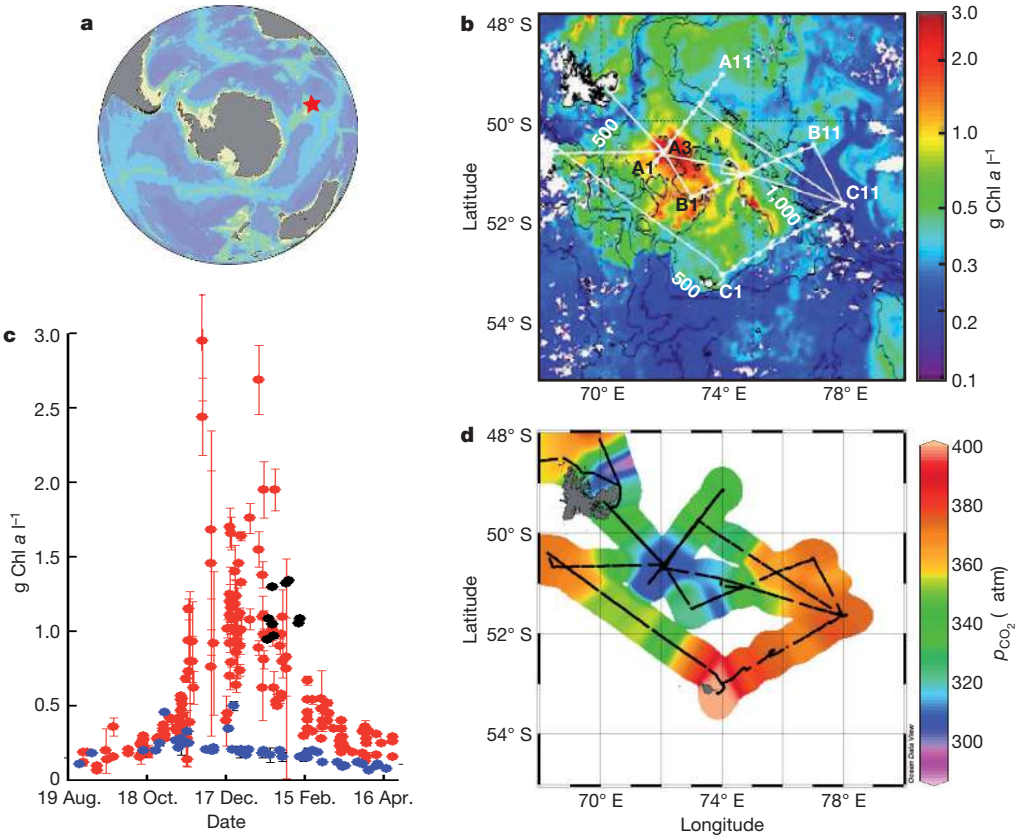

Figure 1 | Location of the study sites, temporal evolution of the bloom and surface water properties. **a**, Location of the Kerguelen plateau (red star) in the Southern Ocean. **b**, Satellite image of the bloom during the KEOPS cruise. The track of the cruise (white line), the position of the stations (white dots) and bathymetry (black lines) are shown. Chl *a*, chlorophyll *a*. **c**, Time series of satellite-determined Chl *a* at stations within the bloom (red dots) and at C11 (blue dots). (MODIS results provided by CSIRO Marine Research, Hobart.) Error bars, ±1 s.d. calculated from the individual passes of the satellite. Black dots denote high-performance liquid chromatography measurements in surface waters during the cruise. **d**, Surface p_{CO_2} measured by underway sampling.

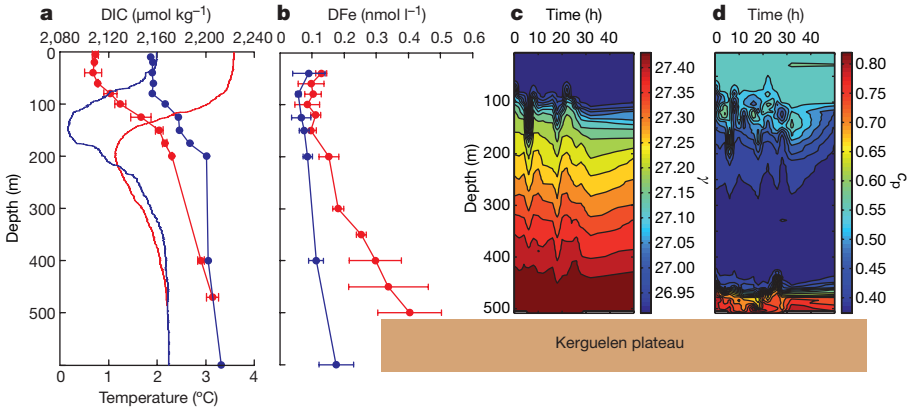

Figure 2 | Iron fertilization above the plateau. **a**, Mean profiles ($n = 3$) of DIC concentrations at A3 (red circles) and at C11 (blue circles). Red and blue lines denote typical temperature profiles at A3 and C11, respectively. Error bars, ±1 s.d. **b**, Mean profiles ($n = 3$) of DFe concentrations at A3 (red circles) and outside the plateau (blue circles). Stations outside the plateau are C11, C9, B11, B9, A11 and A9. Error bars, ±1 s.d. Above the Kerguelen plateau, close to the bottom, a large variability of the vertical DFe gradients among the different profiles was observed, resulting in the large s.d. of the mean DFe value. **c**, Time series of vertical profiles of γ at station A3 (γ = water density − 10^3, where water density is in kg m^{-3}). **d**, Time series of vertical profiles of particle attenuation at 660 nm (c_p) at station A3. A cast was performed every two hours. The brown block labelled Kerguelen plateau represents the bottom at station A3.

the plateau, in comparison to surrounding waters, of 204 ± 77 nmol m^{-2} d^{-1}. This is a maximum estimate of the excess DFe supply, in that it assumes no additional supply to balance the demand at C11 as the demand was not determined at that location (Table 1).

Carbon dioxide uptake fuelled by the enhanced iron supply is clear from the lowered p_{CO_2} of surface waters (Fig. 1d), but how much carbon is exported from surface waters and sequestered at depth? We estimated carbon export using the deficit of ^{234}Th activity in the water column, and the ratio of particulate organic carbon (POC) to ^{234}Th (Fig. 3; Table 1).

The POC export indicated by the ^{234}Th technique in the bloom over the plateau was approximately twice as large as in the HNLC waters off the plateau (Table 1), but still within the range of POC fluxes from the mixed layer estimated in the same way for blooms in the Polar Frontal Zone[25]. At A3, the POC export flux represented about 30% of primary production. The mean excess of carbon export at A3 compared to C11 was 10.8 ± 4.9 and 14.2 ± 7.9 mmol m^{-2} d^{-1} at 100 and 200 m, respectively. This can be compared to the results of SOFEX, the only Southern Ocean iron addition experiment that has measured enhanced POC export[26]. The excess measured at 100 m was 7.1 mmol m^{-2} d^{-1}, and extrapolated to 250 m was 3 mmol m^{-2} d^{-1}.

On the basis of the excess of POC export at 200 m and the excess of DFe supply, we obtain a sequestration efficiency (that is, the excess of POC export divided by the excess of DFe supply) of 70,000 ±

Table 1 | DFe and carbon budget

	DFe		Carbon	
Station	Bloom (A3)	HNLC (C11)	Bloom (A3)	HNLC (C11)
Short-term fluxes*				
Vertical diffusivity (10^{-4} m^2 s^{-1})†	3.2	2.4	3.0	3.8
Vertical gradient (mmol m^{-4})‡	11.2×10^{-7}	2.0×10^{-7}	0.56	0.32
Vertical supply (mmol m^{-2} d^{-1})§	3.1×10^{-5}	0.4×10^{-5}	14.6	10.6
Unaccounted supply (mmol m^{-2} d^{-1})	17.7×10^{-5} ||	ND||	28¶	−2.7¶
Th-derived POC export (mmol m^{-2} d^{-1}) at 100 m#			23.0	12.2
Th-derived POC export (mmol m^{-2} d^{-1}) at 200 m#			24.5	10.3
Seasonal budget*				
Winter concentration (mmol m^{-3})⊗	1.53×10^{-4}	8.6×10^{-5}	2,230	2,237
Summer concentration (mmol m^{-3})**	8.6×10^{-5}	7.2×10^{-5}	2,167	2,214
Winter stock utilization (mmol m^{-2})††	4.7×10^{-3}	9.5×10^{-4}	4,410	1,564
Vertical supply (mmol m^{-2})‡‡	1.4×10^{-3}	1.9×10^{-4}	657	477
Air–sea supply (mmol m^{-2})‡‡			1,260	−121
POC accumulation in the ML (mmol m^{-2})§§			670	190
DOC accumulation in the ML (mmol m^{-2})§§			610	ND
POC export below the ML (mmol m^{-2})||||			5,047	1,730

HNLC, high-nutrient low-chlorophyll; ND, not determined; POC, particulate organic carbon; DOC, dissolved organic carbon; ML, mixed layer.
* See also Supplementary Table 1.
† Mean values corresponding to the depth stratum where the gradient is observed (150–200 m for DFe, and 80–150 m for DIC).
‡ Vertical gradients were determined using the linear part of the vertical profiles (Fig. 2a, b) corresponding to the depth stratum defined in the previous footnote.
§ Vertical supply was calculated by multiplying the vertical gradient with the mean vertical diffusivity coefficient converted to m^2 d^{-1}.
|| This term is the supply of DFe needed to balance the mean net DFe demand (208 nmol m^{-2} d^{-1}) calculated as the difference between the total uptake rate (423 nmol m^{-2} d^{-1}) and the regeneration rate (215 nmol m^{-2} d^{-1}) measured during the cruise. This term was not determined at C11. See text for details.
¶ This term is the mean gas exchange flux calculated from two different parameterizations[31,32] and the wind speed measured during the cruise.
# See text and Methods for details.
⊗ Winter concentration (C_{winter}) was taken from the concentration measured at the depth of the temperature minimum characterizing the remnant winter water (Fig. 2a).
** Summer concentration (C_{summer}) was the mean value measured within the mixed layer during the KEOPS survey.
†† Seasonal apparent consumption was calculated using the equation ($C_{winter} - C_{summer}$)MLD. The mean mixed layer depth (MLD) was 70 ± 20 m and 68 ± 13 m at A3 and C11, respectively.
‡‡ Vertical supply and air–sea supply were calculated assuming linear build-up of the gradients over 90 days.
§§ The accumulation of POC and DOC was the difference between the stock in summer and in winter. (no DOC data are available at C11).
|||| POC export = DIC winter stock utilization + DIC vertical supply + DIC air-sea supply − POC accumulation − DOC accumulation. In a similar way to the POC export derived from Th fluxes, we assume that the carbon export at 200 m was roughly the same as just below the MLD.

46,000 mol mol^{-1} above the Kerguelen plateau. To take into account the possible variability in the C export and DFe supply as the season progresses, we also calculated the sequestration efficiency of the natural fertilization based on the seasonal budgets (Table 1). This yields a much higher value of 668,000 mol mol^{-1} (the ratios between the C export and the DFe supply were 9.9×10^5 and 1.5×10^6 at A3 and C11, respectively). It is evident from the individual terms of the budgets (Supplementary Table 1) that the uncertainty on the efficiency estimate is large, but we have investigated three possible biases, as follows. (1) The vertical diffusivity is difficult to constrain. However, the efficiency ratio is only weakly sensitive to its magnitude because the dissolved inorganic carbon (DIC)/DFe ratio of the resupply is similar to that of the export. (2) Our late-summer observations may under-estimate the iron supply, but even the extreme assumption that DFe concentrations over the plateau were much higher earlier in the year (for example, that the 500 m near-bottom DFe value of 0.40 nM at A3 characterized waters at 200 m throughout the rest of the year) still leads to a seasonal sequestration efficiency of 149,000 mol mol^{-1}. (3) The seasonal budget does not include an additional supply from the dissolution of PFe_{litho}. If we applied, over the whole season, the maximum PFe_{litho} dissolution flux determined in the short-term budget, this also leads to a high efficiency ratio of 159,000 mol mol^{-1}. The high efficiencies resulting from the short and seasonal budgets are consistent with our shipboard observations at A3 of C:Fe uptake rate ratios (200,000 $\pm$ 118,000 mol mol^{-1}) and C:Fe contents of phytoplankton cells (227,000 $\pm$ 5,000 mol mol^{-1}).

Our different approaches to estimating the sequestration efficiency give results that range over an order of magnitude, yet all the estimates are at least 10 times higher than the mean efficiency of ~4,300 mol mol^{-1} estimated from SOFEX and other mesoscale iron addition experiments in the Southern Ocean[7]. Our estimates do not include horizontal transport of DIC and DFe, but mixing with waters outside the plateau would tend to supply DIC and remove DFe from the plateau and thus to increase the sequestration efficiency. Our ratio might be biased if a strong decoupling between carbon and iron cycling existed, but our measurements show that, in the bloom, similar percentages of the fixed C (40%) and Fe (50%) were remineralized as DIC and DFe, respectively. Thus the conclusion that natural iron fertilization over the Kerguelen plateau has a high carbon sequestration efficiency is quite robust.

The higher carbon sequestration efficiency of the natural bloom in comparison to mesoscale iron addition experiments derives from differences in both terms of the sequestration efficiency ratio. The excess of carbon export was higher during the KEOPS bloom than SOFEX, probably owing to its later stage of development (Supplementary Materials), and because during SOFEX the end of the bloom was not reached[26]. The addition of DFe occurs slowly and continuously during natural fertilization, whereas purposeful additions of large amounts of iron within a short period lead to the loss of most (80–95%) of the added DFe during mesoscale enrichment experiments[27].

The occurrence of the Kerguelen bloom is contingent on persistent iron fertilization, but nevertheless its duration is due to the concomitant supply of macronutrients from surrounding waters and from below. The KEOPS results are tightly linked to the mode of iron supply, which is different from dust deposition or purposeful additions. Our estimate of carbon sequestration efficiency is important to the evaluation of palaeo hypotheses[9,10] and future climate change scenarios[11] linking iron supply from below with ocean productivity and its influence on atmospheric carbon dioxide. The enrichment of deep water by terrigenous inputs[10] or by the indirect effect of dust deposition[9] has been proposed. The complex interplay between the iron and carbon cycles[28] precludes a direct extrapolation of how much CO_2 will be really removed from the atmosphere following the fertilization of the Southern Ocean from below, but clearly the natural system is extremely sensitive to iron, far more so than suggested by mesoscale iron addition experiments. However, for the reasons presented above, we emphasize that the high sequestration efficiency determined in the Kerguelen bloom should not be taken as an indication that controversial geoengineering CO_2 mitigation proposals[29,30] will be able to obtain high efficiencies.

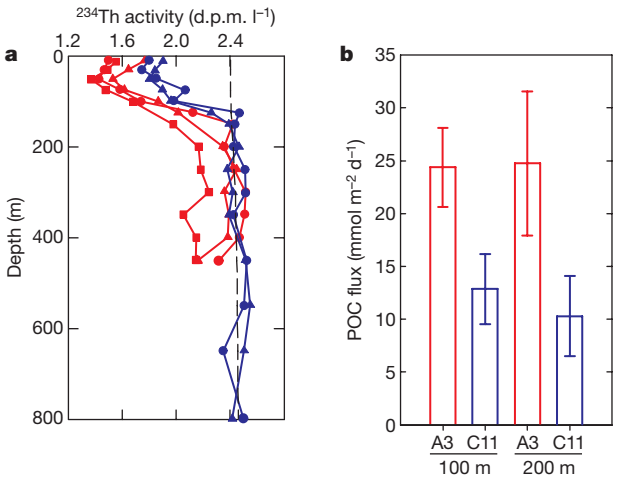

Figure 3 | Carbon export at A3 and C11. **a**, Profiles of ^{234}Th activity at A3 (red lines) and C11 (blue lines). The date of the visits (in 2005) are as follows. At A3; 25 January (circles), 3 February (triangles), 12 February (squares): at C11; 26 January (circles), 05 February (triangles). The dashed line denotes the mean profile of ^{238}U activity. **b**, POC fluxes at A3 and C11. The POC fluxes were derived from ^{234}Th fluxes using a non-steady-state method and POC:^{234}Th ratios (see Methods). The contribution of the vertical diffusivity to the fluxes was negligible at 200 m and around 10% at 100 m, at A3 and C11. The non-steady-state contribution was less than 4% at 100 m. At 200 m it was 34% and 29% at A3 and C11, respectively. Error bars, $\pm$1 s.d. of the total flux. At both depths, POC fluxes were substantially higher inside the bloom compared to outside.

METHODS SUMMARY

Composite images from the satellite-borne MODIS (Moderate Resolution Imaging Spectroradiometer) and MERIS (Medium Resolution Imaging Spectrometer Instrument), processed by ACRI Co. and delivered daily to the RV *Marion Dufresne*, were used to locate the stations inside and outside the bloom. The vessel's seawater supply was used to monitor surface waters. Water column properties were measured *in situ* by instruments mounted on a rosette frame, and discrete samples were collected using Niskin bottles. *In situ* pumps were used to collect particles. All the samples were analysed applying standard protocols. Special attention was paid to Fe sampling and measurements, using trace metal clean techniques.

1. Martin, J. H. Glacial-interglacial CO_2 change: The iron hypothesis. *Paleoceanography* **5**, 1–13 (1990).
2. Brzezinsky, M. A. *et al.* A switch from $Si(OH)_4$ to NO_3^- depletion in the glacial Southern Ocean. *Geophys. Res. Lett.* **29**, doi:10.1029/2001GL014349 (2002).
3. Sigman, D. M. & Boyle, E. A. Glacial/interglacial variations in atmospheric carbon dioxide. *Science* **407**, 859–869 (2000).
4. Bopp, L., Kohfeld, K. E., Le Quéré, C. & Aumont, O. Dust impact on marine biota and atmospheric CO_2 during glacial periods. *Paleoceanography* **18**, doi:10.1029/2002PA000810 (2003).
5. Watson, A. J., Bakker, D. C. E., Ridgwell, A. J., Boyd, P. W. & Law, C. Effect of iron supply on Southern Ocean CO_2 uptake and implications for glacial atmospheric CO_2. *Nature* **407**, 730–733 (2000).
6. Boyd, P. W. *et al.* Mesoscale iron enrichment experiments 1993–2005: Synthesis and future directions. *Science* **315**, 612–617 (2007).
7. De Baar, H. J. W. *et al.* Synthesis of iron fertilization experiments: from the iron age in the age of enlightenment. *J. Geophys. Res.* **110**, doi:10.1029/2004JC002601 (2005).
8. Boyd, P. W., Jackson, G. A. & Waite, A. M. Are mesoscale perturbation experiments in polar waters prone to physical artefacts? Evidence from algal aggregation modelling studies. *Geophys. Res. Lett.* **20**, doi:10.1029/2001GL014210 (2002).

9. Ridgwell, A. J. & Watson, A. Feedback between aeolian dust, climate, and atmospheric CO_2 in glacial time. *Paleoceanogr.* **17,** 1059, doi:10.1029/2001PA000729 (2002).
10. Latimer, J. C. & Filipelli, G. M. Terrigenous input and paleoproductivity in the Southern Ocean. *Paleoceanography* **16,** 627–643 (2001).
11. Jickells, T. D. *et al.* Global iron connections between desert dust, ocean biogeochemistry, and climate. *Science* **308,** 67–71 (2005).
12. Sarmiento, J. L., Hughes, C. W., Stouffer, R. J. & Manabe, S. Simulated response of the ocean carbon cycle to anthropogenic climate warming. *Nature* **393,** 245–249 (1998).
13. Marinov, I., Gnanadesikan, A., Toggweiler, J. R. & Sarmiento, J. L. The Southern Ocean biogeochemical divide. *Nature* **441,** 964–967 (2006).
14. Coale, K. H. *et al.* Southern Ocean iron enrichment experiment: Carbon cycling in high- and low-Si waters. *Science* **304,** 408–414 (2004).
15. Boyd, P. W. *et al.* A mesoscale phytoplankton bloom in the polar Southern Ocean stimulated by iron fertilization. *Nature* **407,** 695–702 (2000).
16. Gervais, F., Riebesell, U. & Gorbunov, M. Y. Change in primary productivity and chlorophyll a response to iron fertilization in the Southern Polar Frontal Zone. *Limnol. Oceanogr.* **47,** 1324–1335 (2002).
17. Hart, T. J. Phytoplankton periodicity in Antarctic surface water. *Discov. Rep.* **VIII,** 1–268 (1942).
18. Sullivan, C. W., Arrigo, K. R., McClain, C. R., Comiso, J. C. & Firestone, J. Distribution of phytoplankton blooms in the Southern Ocean. *Science* **262,** 1832–1837 (1993).
19. Tyrell, T. *et al.* Effect of seafloor depth and phytoplankton blooms in high nitrate low chlorophyll (HNLC) regions. *J. Geophys. Res.* **110,** doi:10.1029/2005JG000041 (2005).
20. Blain, S. *et al.* A biogeochemical study of the island mass effect in the context of the iron hypothesis: Kerguelen Islands, Southern Ocean. *Deep-sea Res. I* **48,** 163–187 (2001).
21. Measures, C. I. & Vink, S. Dissolved Fe in the upper waters of the Pacific sector of the Southern Ocean. *Deep-sea Res. II* **48,** 3913–3941 (2001).
22. Timmermans, K. R. *et al.* Growth rates of large and small Southern Ocean diatoms in relation to availability of iron in natural seawater. *Limnol. Oceanogr.* **46,** 260–266 (2001).
23. Law, C., Abraham, E. R., Watson, A. & Liddicoat, M. Vertical eddy diffusion and nutrient supply to the surface mixed layer of the Antarctic Circumpolar Current. *J. Geophys. Res.* **108,** doi:10.1029/2002JC001604 (2003).
24. Boyd, P. W. *et al.* FeCycle: attempting an iron biogeochemical budget from a mesoscale SF_6 tracer experiment in unperturbated low iron waters. *Glob. Biochem. Cycles* **19,** doi:10.1029/2005GB002494 (2005).
25. Rutgers Van Der Loeff, M. M., Buesseler, K. O., Bathmann, U., Hense, I. & Andrews, J. Comparison of carbon and opal export rates between summer and spring bloom in the region of the Antarctic Polar Front, SE Atlantic. *Deep-sea Res. II* **49,** 3849–3869 (2002).
26. Buesseler, K. O., Andrews, J. E., Pike, S. M. & Charette, M. A. The effects of iron fertilization on carbon sequestration in the Southern Ocean. *Science* **304,** 414–417 (2004).
27. Bowie, A. R. *et al.* The fate of added iron during a mesoscale fertilisation experiment in the Southern Ocean. *Deep-sea Res. II* **48,** 2703–2743 (2001).
28. Gnanadesikan, A., Sarmiento, J. L. & Slater, R. D. Effects of patchy ocean fertilization on atmospheric carbon dioxide and biological production. *Glob. Biochem. Cycles* **17,** doi:10.1029/2002GB001940 (2003).
29. Buesseler, K. O. & Boyd, P. W. Will ocean fertilization work? *Science* **300,** 67–68 (2003).
30. Chisholm, S. W., Falkowski, P. G. & Cullen, J. J. Dis-crediting ocean fertilization. *Science* **294,** 309–310 (2001).
31. Wanninkhof, R. H. & McGillis, W. R. A cubic relationship between air-sea exchange and wind speed. *Geophys. Res. Lett.* **26,** 1889–1892 (1999).
32. Nightingale, P. *et al. In situ* elevation of the sea-air gas exchange parameterisations using novel conservative and volatile tracers. *Glob. Biochem. Cycles* **14,** 373–387 (2000).

Acknowledgements We thank the captain and the crew of the RV *Marion Dufresne*. This work was supported by the Institut National des Sciences de L'Univers (INSU) and the Centre National de la Recherche Scientifique (CNRS), l'Institut Paul Emile Victor (IPEV), French-Australian Science and Technology (FAST), the Australian Commonwealth Cooperative Research Centre programme through the Antarctic Climate and Ecosystem CRC, and Belgian Science Policy (BELSPO). The project benefited from collaboration with N. Metzl, leader of Ocean Indien Service d'Observation (OISO) supported by INSU, IPEV and Institut Pierre Simon Laplace (IPSL). We acknowledge the contributions of V. Barthaux, P. Catala, J. Caparros and J. Raz (technical assistance), and M.P. Jouandet (computation of the seasonal carbon budget).

Author Information Reprints and permissions information is available at www.nature.com/reprints. The authors declare no competing financial interests. Correspondence and requests for materials should be addressed to S.B. (stephane.blain@univmed.fr).

METHODS

Selection of stations and hydrographic sampling. Composite images of MODIS and MERIS processed by ACRI Co. and delivered daily to the RV *Marion Dufresne* were used to locate the stations inside and outside the bloom. The vessel seawater supply (intake at a depth of 5 m) was used to continuously monitor p_{CO_2}, DIC, temperature, salinity and fluorescence[33]. Vertical sampling of the water column from the surface to the bottom was performed using 22 acid-cleaned 12-l Niskin bottles mounted on a CTD rosette system with a lowered acoustic Doppler current profiler (LADCP) and a C star transmissiometer (WETLABS). Clean trace metal samples were obtained using ten 12-l Go-Flo bottles mounted on a 2,500-m Kevlar line and trigged by Teflon messengers. *In situ* pumps were used to collect particles. The vertical diffusivity, K_z, was estimated from the vertical density profiles and from corresponding Thorpe scales[34,35].

Biogeochemical parameters. Dissolved iron[36] and organic ligands[37] present in filtered (<0.2 μm) sea water were measured on board in a clean laboratory. The accuracy of DFe determinations was checked using the new sub-nanomolar Fe standard sampled and analysed during the SAFE cruise[38]. Samples from Go-Flo bottles were filtered (>0.2 μm) for particulate trace metal determinations[39]. The crustal ratio PFe/PAl = 0.2 (ref. 40) was used to estimate PFe_{lith}. Discrete water samples taken from Niskin bottles were analysed for macronutrients[41], DIC[33], DOC, POC[41], and U/Th β-counting[42]. Rates of production were determined using 24-h deck incubations with simulated *in situ* light levels, using ^{13}C (ref. 41). Uptake and regeneration rates of iron were determined using ^{55}Fe and a biogenic budget[27]. The net iron demand was calculated as the difference between the total biogenic demand and supply. Gross community production and community respiration were concurrently determined by O_2 and DIC evolution using 24-h incubations with simulated light levels[43]. ^{234}Th export fluxes at 100 m and 200 m depth were estimated using a non-steady-state (NSS) one-dimensional model accounting for vertical diffusion (equations in ref. 44). ^{234}Th fluxes at A3 were 2,999 and 5,217 d.p.m. m^{-2} d^{-1} at 100 and 200 m, respectively, and at C11, 2,003 and 2,281 d.p.m. m^{-2} d^{-1} at 100 and 200 m, respectively. Conversion to POC export was based on POC/^{234}Th (C/Th) ratios of 5–210-μm particles from large volume filtrations at 100 m depth (7.7 and 6.1 μmol d.p.m.$^{-1}$ at A3 and C11, respectively). Estimates at 200 m depth were based on C/Th from 1–335-μm particles from free-drifting sediment trap collections at site A3 (4.7 μmol d.p.m.$^{-1}$) and on C/Th ratios from 5–210-μm particles from large volume filtrations at 130 m depth at C11 (4.5 μmol d.p.m.$^{-1}$).

33. Jabaud, A., Metzl, N., Brunet, C., Poisson, A. & Schauer, B. Interannual variability of the carbon dioxide system in the Southern Indian Ocean (20°S-60°S): the impact of a warm anomaly in austral summer. *Glob. Biochem. Cycles* **18,** doi:10.1029/2002GB002017 (2004).
34. Osborn, T. R. Estimate of vertical diffusion from dissipation measurements. *J. Phys. Oceanogr.* **10,** 83–89 (1980).
35. Dillon, T. M. Vertical overturns: a comparison of Thorpe and Ozmidov length scales. *J. Geophys. Res.* **85,** 9601–9613 (1982).
36. Sarthou, G. *et al.* Atmospheric iron deposition and sea-surface dissolved iron concentrations in the eastern Atlantic Ocean. *Deep-Sea Res. I* **50,** 1339–1352 (2003).
37. Croot, P. & Johansson, M. Determination of iron speciation by cathodic stripping voltammetry in seawater using the competing ligand 2-(2-thiazolylazo-*p*-cresol (TAC). *Electroanalysis* **12,** 565–576 (2000).
38. Johnson, K. S. *et al.* Sampling and analysis of Fe: The SAFE iron intercomparison cruise. *Eos Trans. AGU* 87(36), Ocean Sci. Meet. Suppl. (2006).
39. Cullen, J. T. & Sherrel, M. Techniques for determination of trace metal in small samples of size-fractionated particulate matter: phytoplankton metals off central California. *Mar. Chem.* **67,** 233–247 (1999).
40. Wedepohl, K. H. The composition of continental crust. *Geochim. Cosmochim. Acta* **59,** 1217–1232 (1995).
41. Fernandez, C., Raimbault, P., Caniaux, Y., Garcia, N. & Rimmelin, P. An estimation of annual new production and carbon budget in the northeast Atlantic Ocean during 2001. *J. Geophys. Res.* **110,** doi:10.1029/2004JC002621 (2005).
42. Pike, S. M., Buesseler, K. O., Andrews, J. & Savoye, N. Quantification of ^{234}Th recovery in small volume of sea water samples by inductively coupled plasma-mass spectrometry. *J. Radioanal. Nucl. Chem.* **263,** 355–360 (2005).
43. Robinson, C. & Williams, P. J. I. Plankton net community production and dark respiration in the Arabian Sea during September 1994. *Deep-Sea Res. II* **46,** 745–765 (1999).
44. Savoye, N. *et al.* ^{234}Th sorption and export models in the water column: a review. *Mar. Chem.* **100,** 234–249 (2006).

Supplementary discussion

Ecosystem structure

A major difference between KEOPS and previous mesoscale iron addition experiments is the longer duration of the Kerguelen bloom. During the survey, we encountered an ecosystem that had evolved over roughly two months, thus revealing a higher degree of maturation than those observed in previous short-term studies. This resulted in distinct features in the taxonomic composition and the contribution of the major components of the planktonic food web associated with the Kerguelen bloom.

Diatoms dominated the phytoplankton community in terms of carbon biomass at both the A3 and C11 stations (Supplementary Table 2), but the activity and composition of the autotrophic communities were substantially different. On the plateau at A3, photosynthetic efficiency (Fv/Fm) was 0.55, a typical value for the phytoplankton community in an iron fertilised patch[1]. Large cells (>10µm) accounted for 79%, 72%, 67% of the integrated primary production, nitrate uptake, ammonium uptake, respectively. By contrast, at C11 Fv/Fm was 0.3 and large cell contributions were only 34%, 11%, 37% of the respective uptake fluxes. At A3, two chain-forming diatom taxa, small *Chaetoceros* spp. (*Hyalochaete*) and large *Eucampia antarctica*, dominated diatom cell abundance and diatom carbon biomass, respectively (Supplementary Table 3). In contrast, at C11 the very small diatom, *Fragilariopsis pseudonana,* dominated diatom abundance but the open-ocean species *Fragilariopsis kerguelensis,* dominated diatom carbon biomass at this location. The minor contribution of *F. kerguelensis* at A3 contrasts strongly with its dominance during Southern Ocean mesoscale iron additions[2]. *Chaetoceros Hyalochaete* blooms have been observed in mesoscale iron addition experiments in the subarctic Pacific, with *Chaetoceros debilis* responsible for the massive iron-mediated bloom during SEEDS[3], and *Chaetoceros* spp. forming an early bloom and later decline during SERIES [4]. Floristic succession was also observed at A3 with the loss of the smaller *Chaetoceros* spp. *Hyalochaete* and the

development of a monopolising *Eucampia antarctica* abundance apex towards the end of the bloom (Supplementary Table 3).

The abundance of heterotrophic bacteria at Station A3 was roughly twice that observed at C11, an enrichment that falls at the higher end of values reported for mesoscale iron additions[1, 3, 5]. By contrast, we observed similar abundances of heterotrophic nanoflagellates and ciliates within and outside the bloom. This observation contrasts results from previous studies where heterotrophic nanoflagellates[6] and ciliates[1] rapidly responded to deliberate iron enrichment. Grazing by heterotrophic nanoflagellates accounted for only ≈ 35% of bacterial biomass production at Station A3, while at Station C11 flagellates controlled bacterial production (by ≈ 95%). The higher viral abundances (2.8-fold) and viral production rates (7-fold) at A3 than at C11 indicate that viruses had an important role in the regulation of bacterial biomass and thus the cycling of carbon and most likely iron within the Kerguelen bloom[7].

Mesozooplankton biomass was substantially higher above the Kerguelen plateau (by a factor of 3) than at Station C11 (Supplementary Table 1), a result that clearly distinguishes the present from previous studies where no response of mesozooplankton to deliberate iron enrichment was detectable. At the bloom Station A3, mesozooplankton grazing accounted for 52±18 % of integrated primary production. The dominant taxons were medium size calanoids (mainly copepodite stages), Oithonidae and pteropods. This is similar to the distribution pattern found in the bloom over the shelf of South Georgia [8]. Evidence of the omnivory of Oithonidae has been demonstrated [9, 10] suggesting that top-down control on microzooplankton could be important above the Kerguelen Plateau.

Supplementary Table 1: uncertainties of the basic terms of the DFe and carbon budgets.

	DFe		Carbon	
Station	Bloom (A3)	HNLC(C11)	Bloom(A3)	HNLC(C11)
Mixed layer depth (%)[a]	29	30	29	30
Summer concentration (%)	38[b]	20[c]	2.7[d]	0.8[d]
Winter concentration (%)	20[e]	20[f]	2[e]	2[f]
Flux CO_2 from the atmosphere (%) [g]			18	18
POC (%) [h]			4	12
DOC (%) [i]			6	
Th derived POC export at 100m (%) [j]			15	15
Th derived POC export at 200m (%) [j]			27	36
Range of vertical diffusivity (10^{-4} m^2 s^{-1}) [k]	0.1-27	0.20-5.4	0.55-5.1	0.58-11
Range for the duration of the bloom (d) [l]	75-105	75-105	75-105	75-105

(a) Relative standard deviation, n=37 at A3 and n=14 at C11.

(b) Relative standard deviation, n=33 corresponding to the samples in the surface mixed layer at the stations above the plateau.

(c) Relative standard deviation, n=9 corresponding to the samples in the surface mixed layer at the stations outside the plateau.

(d) Relative standard deviation, At A3, n=10 corresponding to the samples in surface mixed layer at the different visits. n=3 at C11.

(e) Relative standard deviation, n=3 corresponding to the samples in the winter water at the different visits.

(f) Relative standard deviation. The value of A3 is reported because there was only one profile at C11.

(g) Estimated from two different parameterisations [11, 12]

(h) Relative standard deviation, n=3 corresponding to the different profiles at A3 and C11.

(i) Relative standard deviation, n=3 corresponding to the different visits at A3.

(j) Relative standard deviation, calculated from uncertainties of analytical measurements on 234Th counting and POC/Th measurements (n=1 except for POC/Th in the trap n=3).

(k) Resulting from the analysis of n= 11 and n=8 vertical profiles at A3 and C11, respectively.

(l) Estimated from Fig. 1c.

Supplementary Table 2.

Carbon biomass of major components of the plankton community.

	A3 first visit (19/01)	A3 last visit (12/02)	C11 (26/01)
Autotrophs	mg C m^{-2} [(b)]	mg C m^{-2} [(b)]	mg C m^{-2} [(b)]
Diatoms	4,724 [(c)]	3,777 [(c)]	1,852 [(c)]
Nanoflagellates	161	302	824
Heterotrophs			
Bacteria	492	569	278
Nanoflagellates	735	293	401
Ciliates	50	50	36
Mesozooplankton[(d)]	mg C m^{-2} [(d)]	mg C m^{-2} [(d)]	mg C m^{-2} [(d) (e)]
330-500 µm	870	323	292
500-1,000 µm	2,290	1,672	968
1,000-2,000 µm	4,080	3,709	1,569
> 2,000 µm	3,570	3,200	338
Total	10,810	8,904	3,167

[(a)]Abundances of diatoms, nanoflagellates and ciliates are based on microscopic observations and heterotrophic bacteria were enumerated by flow cytometry. Conversion to carbon biomass was done using conversion factors from the literature [13-15]. Mesozooplankton were collected from vertical hauls (330 µm) and enumerated by automatic optical counting [16]. The taxonomic identifications were made by optical observations and conversion factors [17] were applied to obtain mesozooplankton carbon biomass.

[(b)]Integrated over mixed layer depth.

[(c)]Calculated for living cells that represent 83%, 84% and 64.4% of the total cells, respectively.

[(d)]Integrated over 200m.

[(e)]Based on sample collected on 22/01.

Supplementary Table 3.

Contribution of major diatom species at A3 and C11

	Abundance (%)			Biomass (%)		
Species	A3[a]	A3[b]	C11[c]	A3[a]	A3[b]	C11[c]
Chaetoceros spp. (*Hyalochaete*)	56.3	0.2	0	17.4	-	-
Chaetoceros resting spores (*Hyalochaete*)	0	0.04	0.01	-	-	-
Eucampia antarctica	11	64	0	38	72.9	-
Fragilariopsis kerguelensis	5.0	2.7	4.2	5.5	1.8	49.4
Fragilariopsis pseudonana	0.3	0.2	55.7	-	-	35.1
Thalassionema nitzschioides	5.9	1.6	0.15	1.5	0.2	0.14
Thalassiosira lentiginosa	0.1	0.1	0.04	-	0.06	0.06

[a] Sample collected at 50m during the first visit at A3 (19/01).

[b] Sample collected at 60m during the last visit at A3 (12/02)

[c] Sample collected at 60 m during the first visit at C11(26/01)

Supplementary References.

1. Boyd, P. W. et al. A mesoscale phytoplankton bloom in the polar Southern Ocean stimulated by iron fertilization. *Nature* **407**, 695-702 (2000).
2. Gall, M. P., Boyd, P. W., Hall, J., Safi, K. A. & Chang, H. Phytoplankton processes. Part 1: Community structure during the Southern Ocean Iron RElease Experiment (SOIREE). *Deep-Sea Res. II* **48**, 2551-2570 (2001).
3. Tsuda, A. et al. A Mesoscale Iron Enrichment in the Western Subarctic Pacific Induces a Large Centric Diatom Bloom. *Science* **300**, 958-961 (2003).
4. Boyd, P. W. et al. The evolution and termination of an iron-induced mesoscale bloom in the northeast subarctic Pacific. *Limnol. Oceanogr.* **50**, 1872-1886 (2005).
5. Boyd, P. Ironing Out Algal Issues in the Southern Ocean. *Science* **304**, 396-397 (2004).
6. Saito, H. et al. Response of microzooplankton to in situ iron fertilization in the western subarctic Pacific (SEEDS). *Prog. Oceanogr.* **64**, 223-236 (2005).
7. Fuhrman, J. A. Marine viruses and their biogeochemical and ecological effects. *Nature* **399**, 541-548 (1999).
8. Atkinson, A. et al. Zooplankton response to a phytoplankton bloom near South Georgia, Antarctica. *Mar. Ecol. Prog. Ser.* **144**, 195-210 (1996).
9. Schmidt, K. et al. Trophic relationships among Southern Ocean copepods and krill: some uses and limitations of a stable isotope approach. *Limnol. Oceanogr.* **48**, 277-289 (2003).

10. Smetacek, V., Assmy, P. & Henjes, J. The role of grazing in structuring Southern Ocean pelagic ecosystems and biogeochemical cycles. *Antarct. Sci.* **16**, 541-558 (2004).

11. Wanninkhof, R. H. & McGillis, W. R. A cubic relationship between air-sea exchange and wind speed. *Geophys. Res. Lett.* **26**, 1889-1892 (1999).

12. Nightingale, P. et al. In situ elevation of the sea-air gas exchange parameterisations using novel conservative and volatile tracers. *Glob. Biochem. Cycles* **14**, 373-387 (2000).

13. Fukuda, R., Ogawa, H., Nagata, T. & Koike, I. Direct determination of carbon and nitrogen contents of natural bacterial assemblage in marine environments. *Appl. Environ. Microbiol.* **64**, 3352-3358 (1998).

14. Borsheim, K. Y. & Bratak, G. Cell volume to cell carbon conversion factors for a bacterivorous Monas sp. enriched from sea water. *Mar. Ecol. Prog. Ser.* **36**, 171-179 (1987).

15. Putt, M. & Stoecker, D. K. An experimentally determined carbon: volume ratio for marine "oligotrichous" ciliates from estuarine and coastal waters. *Limnol. Oceanogr.* **34**, 1097-1103 (1989).

16. Beaulieu, S. E. et al. Using an optical plankton counter to determine the size distributions of preserved zooplankton samples. *J. Plank. Res.* **21**, 1939-1956 (1999).

17. Riandey, V., Champalbert, G., Carlotti, F., Taupier-Letage, I. & Thibault-Botha, D. Zooplankton distribution related to the hydrodynamic features in the Algerian Basin (western Mediterranean Sea) in summer 1997. *Deep-Sea Res. I* **52**, 2029-2048.

Supplementary Figure 1

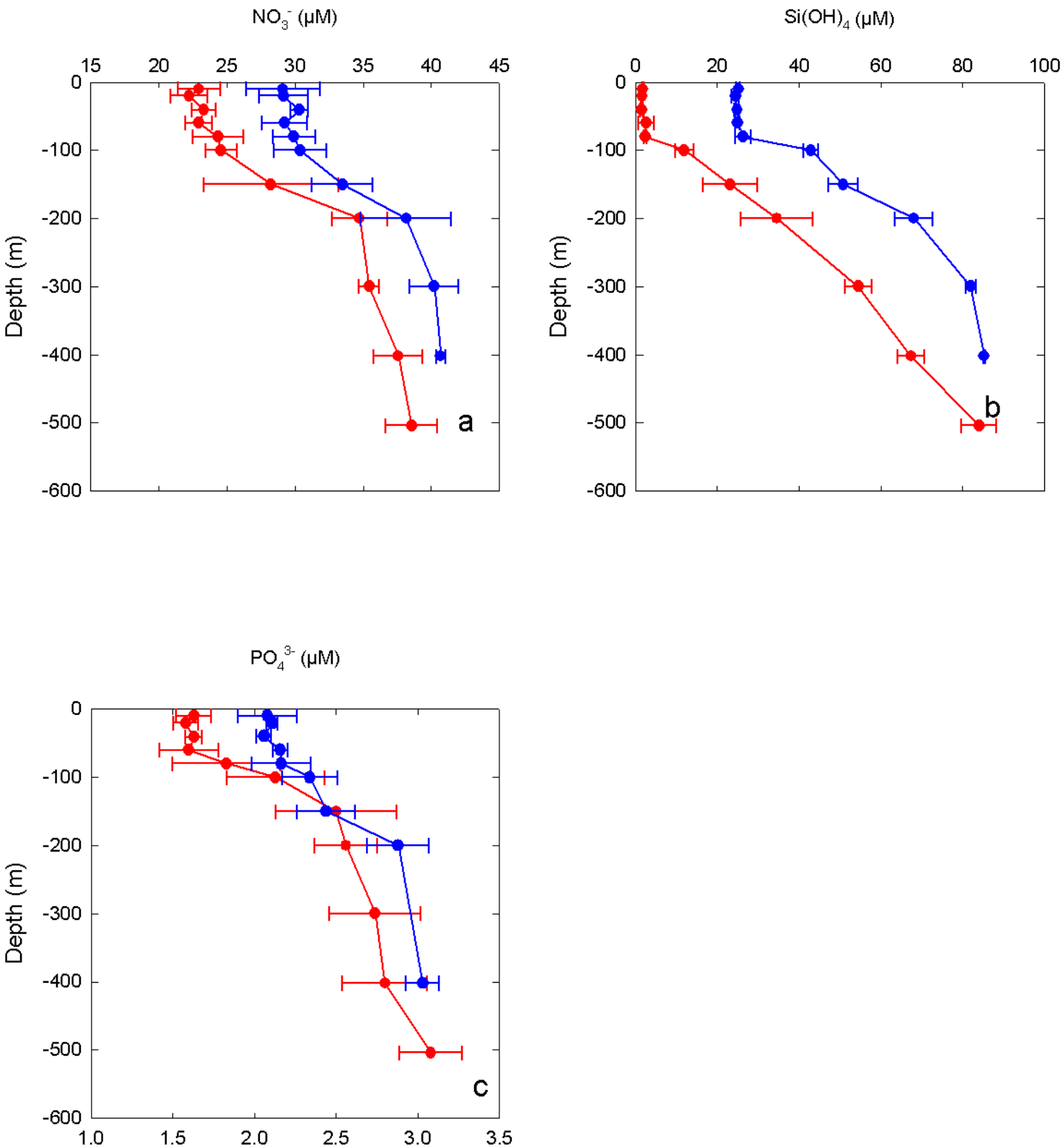

legend of the figure : mean profiles at station A3 (red) and C11 (blue).
The error bar is +/- one standard deviaton.